

# PURE-LET Image Deconvolution

Jizhou Li, *Student Member, IEEE*, Florian Luisier, *Member, IEEE*, and Thierry Blu, *Fellow, IEEE*

**Abstract**—We propose a non-iterative image deconvolution algorithm for data corrupted by Poisson or mixed Poisson-Gaussian noise. Many applications involve such a problem, ranging from astronomical to biological imaging. We parametrize the deconvolution process as a linear combination of elementary functions, termed as linear expansion of thresholds (LET). This parametrization is then optimized by minimizing a robust estimate of the true mean squared error, the Poisson unbiased risk estimate (PURE). Each elementary function consists of a Wiener filtering followed by a pointwise thresholding of undecimated Haar wavelet coefficients. In contrast to existing approaches, the proposed algorithm merely amounts to solving a linear system of equations which has a fast and exact solution. Simulation experiments over different types of convolution kernels and various noise levels indicate that the proposed method outperforms state-of-the-art techniques, in terms of both restoration quality and computational complexity. Finally, we present some results on real confocal fluorescence microscopy images, and demonstrate the potential applicability of the proposed method for improving the quality of these images.

**Index Terms**—Image deconvolution, Poisson noise, mixed Poisson-Gaussian noise, unbiased risk estimate, MSE estimation, fluorescence microscopy.

## I. INTRODUCTION

**I**MAGE deconvolution intends to restore the underlying image from measurements that are degraded by a linear blurring operator and further corrupted by noise. Blurring is usually caused by the physical low-pass behaviour of optical systems, which brings an immediate loss of resolution. Two predominant sources of noise are often considered during the acquisition process [1], [2]. One is caused by the intrinsic thermal and electronic fluctuations of the acquisition devices, which is usually modeled as additive-white-Gaussian-noise (AWGN). The other one is due to fluctuations in the number of detected photons and is an inherent limitation of the detection process occurring in photosensitive devices, such as the photomultiplier tube (PMT), photodiodes and charge-coupled device (CCD) cameras. This happens typically in adverse conditions such as poorly illuminated environments or short exposure times. In the context of photon-counting, the noise model follows a Poisson statistics which is strongly signal-dependent. In the case of images acquired with CCD cameras, it is reasonable to consider the noise as a mixed Poisson-Gaussian model [3]–[5]. Astronomy [4], [6], [7], medicine [3], [8], [9] and biology [10]–[16] are typical applications where low-intensity signals are frequently encountered.

This work was supported in part by grants from the Research Grants Council (RGC) of Hong Kong (AoE/M-05/12).

J. Li and T. Blu are with the Department of Electronic Engineering, the Chinese University of Hong Kong, Shatin, N.T., Hong Kong (e-mail: jzli@ee.cuhk.edu.hk; thierry.blu@m4x.org).

F. Luisier is with Roche Diagnostics Hematology, Boston, MA (e-mail: florian.luisier@roche.com).

## A. Overview of Related Works

Many efficient image restoration algorithms have been designed under the additive (and often white) Gaussian noise assumption [17]–[21]. However, these approaches become sub-optimal when estimating the underlying intensities of Poisson random variables, potentially further degraded by independent AWGN. This is due to the signal-dependent nature of Poisson noise; i.e., the noise variance in each pixel is proportional to the intensity of the underlying signal. The development of deconvolution algorithms specifically designed for this scenario then becomes essential [22]–[24].

In the presence of Poisson noise, a popular method is the Richardson-Lucy (RL) algorithm [25], [26], see [10], [14], [27] for a comprehensive review. The RL algorithm can be understood as a maximum-likelihood (ML) estimate, and has been used extensively in many applications thanks to its accounting of the Poisson statistics. However, this algorithm will amplify noise after a few iterations due to the ill-posedness of the deconvolution problem. Instead, many authors adopt the optimization framework of an objective function consisting of a data term, which quantifies the proximity between the estimated image and the measurement, plus a convex non-smooth regularizer. In this framework, several different regularizers are used such as total-variation [28]–[30], wavelet-based [31]–[34]. However, the Poisson log-likelihood is non-quadratic (but convex), which often requires the application of relatively sophisticated optimization theory [22]. Some further works adopt modified RL algorithm and were proposed to improve the computational efficiency [13], [15], [22], [29], [35]–[37]. For example, Figueiredo *et al.* [22] proposed to use the alternating direction method of multipliers to solve the optimization problem, Setzer *et al.* [35] employed the split Bregman technique, and Pustelnik *et al.* [36] proposed a parallel proximal algorithm based on the use of hybrid regularization techniques.

Apart from these works, [23] employed a class of second-order derivative-based regularizers. Dupé *et al.* [38] proposed a frame-based method using the Anscombe variance stabilizing transform (VST), which changes the linear degradation model with Poisson noise into a nonlinear model with additive Gaussian noise. However, as pointed out in [29], [39], such approximations are inaccurate when the observed number of photons is small and are not really well suited to deconvolution. Similar to the Anscombe transform but with quite different mathematical basis, Rond *et al.* [40] introduced a Plug-and-Play framework to integrate the existing Gaussian solvers to Poisson noise problems. Finally, we should mention a dictionary learning approach [41], which involves a sparse representation over a learned dictionary.

In the context of mixed Poisson-Gaussian noise, there has

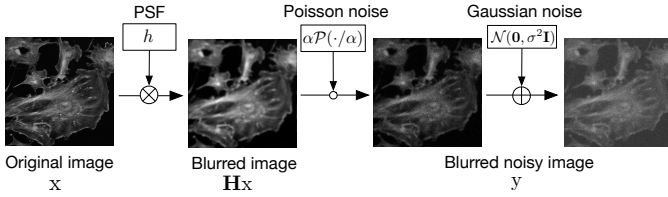


Fig. 1. Linear image degradation model caused by blurring and noise. Note that this model includes both the Poisson noise case ( $\sigma^2 = 0$ ) and the mixed Poisson-Gaussian noise case ( $\sigma^2 \neq 0$ ). Image deconvolution is to restore the original image  $x$  from the blurred noisy image  $y$ .

been a growing interest in noise identification problems [1], [42], as well as denoising problems [2], [43]–[45]. However, the literature on deconvolution problems under this noise hypothesis is limited despite its importance [4], [46]–[50]. Among existing works, a weighted squared  $\ell_2$  norm noise approximation was proposed in [47], a primal-dual proximal splitting algorithm was proposed in [48] by investigating the properties of the Poisson-Gaussian log-likelihood, and more recently Marnissi *et al.* [50] proposed a variational Bayesian approach for this problem.

In most of the above deconvolution approaches, a regularization parameter plays an important role in the quality of the recovery image, balancing the tradeoff between data-fidelity and regularization terms. This value needs to be tuned manually for obtaining the optimal solutions for different scenarios. This process is both time consuming, since it needs to solve the minimization problem several times, and unrealistic in practice. To solve this issue, there are some approaches for the automatic parameter selection including generalized cross validation (GCV) [38], [51], the discrepancy principle [34], [52]–[55]. However, these criteria have many local minima in general, thus an inaccurate estimate of the termination point can result in a solution whose relative error is significantly higher than the optimal value.

## B. Contributions

The major contribution of this paper is to extend the SURE-LET deconvolution approach introduced in [21] to the Poisson and mixed Poisson-Gaussian noise cases. We also present the deconvolution results on real confocal fluorescence microscopy images.

The proposed approach has several advantages over other existing techniques: 1) It is non-iterative and thus has an explicit solution; 2) It is a parameter-free method; 3) It has low computational complexity since it boils down to solving a small linear system of equations; 4) It favorably compares to state-of-the-art techniques, in terms of both restoration quality and computational time. In details, our method consists in approximating the deconvolution process as a linear combination of elementary processings of the image, termed “linear expansion of thresholds (LET)” whose coefficients are obtained by minimizing a quadratic criterion (typically, the mean-squared error/MSE, or its statistical estimate) [2], [21], [56], [57]. In the present paper, each elementary processing consists of Wiener filtering followed by wavelet-domain

thresholding. We derive a theoretically unbiased estimate of the MSE, the Poisson unbiased risk estimate (PURE), and use it to optimize the coefficients of the LETs. Note that thanks to the linear representation of the LET processing, this transform-domain optimization step is actually performed in the image-domain [56], [58].

Compared to a Maximum A Posteriori (MAP) approach, PURE minimization is akin to Bayesian Least Squares (BLS) because the PURE is essentially a proxy for the MSE. And, indeed, minimizing the MSE  $\mathbb{E}\{\|\hat{x}(y) - x\|^2\}$  over all functions  $\hat{x}$  of  $y$ , results in the conditional expectation  $\hat{x}_{\text{BLS}}(y) = \int x p(x|y) dx$ , which involves the posterior pdf  $p(x|y)$  directly [59]. On the other hand, the MAP solution  $\hat{x}_{\text{MAP}}(y) = \arg \max_x p(x|y)$  results from the maximization of this posterior. It should be obvious that, when  $p(x|y)$  is a very localized function of  $x$ , the two expressions should not differ significantly. The most important difference between the two approaches is that, contrary to the MAP which requires a prior knowledge of the statistics of  $x$ , the Bayesian Least Squares solution can be estimated without such a knowledge by using the PURE as a (very accurate) statistical approximation of the MSE.

The rest of the paper is organized as follows. In Section II, we introduce the theoretical basis of this work, specifically the LET framework and PURE for deconvolution problem with Poisson and mixed Poisson-Gaussian noises. Then we provide a typical structure of the elementary functions in Section III. In Section IV, we compare the proposed method on synthetic data with several state-of-the-art techniques under various noise levels and different types of convolution kernels. We show an application to real confocal fluorescence microscopy images in Section V. Some conclusions are drawn in Section VI.

## II. THEORETICAL BACKGROUND

### A. Problem Statement

One general observation model is shown in Fig. 1. The first noise component is signal-dependent, and follows a Poisson distribution whose mean depends on the true image intensity. The second one, accounting for detector noise, is modeled as a Gaussian random variable of mean zero and variance  $\sigma^2$ . Mathematically, this model is given by

$$y = \alpha \mathcal{P}\left(\frac{\mathbf{H}x}{\alpha}\right) + \mathcal{N}(\mathbf{0}, \sigma^2 \text{Id}), \quad (1)$$

where  $y \in \mathbb{R}^N$  denotes the distorted observation of the unknown  $d$ -dimensional true image  $x \in \mathbb{R}^N$ ,  $N = N_1 \times N_2 \times \dots \times N_d$ .  $\mathbf{H} \in \mathbb{R}^{N \times N}$  implements a convolution of the point spread function (PSF)  $h$ . We need  $\mathbf{H}x \in \mathbb{R}^N$  to ensure the inherently non-negativity of Poisson intensities.  $\mathcal{P}(\cdot)$  represents the effect of Poisson noise and  $\alpha \in \mathbb{R}_+$  is the scaling factor, which controls the strength of noise. Specifically, larger values of  $\alpha$  will lead to lower intensity images and thus higher Poisson noise.  $\sigma^2$  is the variance of AWGN.

Note that it is possible to simplify the general model in (1) depending on the application. For instance, a purely Poissonian

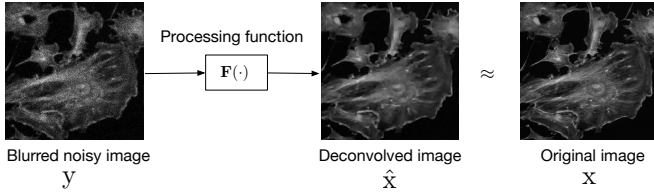


Fig. 2. The restoration process amounts to finding the processing function  $\mathbf{F}(\cdot)$  that minimizes the difference between  $\hat{x}$  and  $x$ .

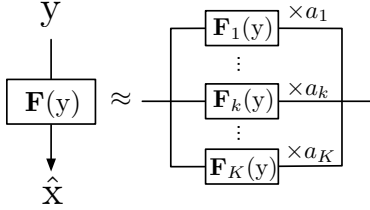


Fig. 3. The LET idea: the processing  $\mathbf{F}$  is approximated by a linear combination of few elementary functions  $\mathbf{F} = \sum_{k=1}^K a_k \mathbf{F}_k$ . In that setting, the restoration process amounts to finding the  $K$  coefficients  $a_1, a_2, \dots, a_K$ .

model is a special case, and can be obtained when  $\sigma^2 = 0$  as in [23], [29], [60]

$$y = \alpha \mathcal{P} \left( \frac{\mathbf{H}x}{\alpha} \right). \quad (2)$$

Because the random variable  $\alpha \mathcal{P} \left( \frac{\mathbf{H}x}{\alpha} \right)$  converges in law to the deterministic value  $\mathbf{H}x$  when  $\alpha \rightarrow 0$ , this model becomes the classical Gaussian noise case  $y = \mathbf{H}x + \mathcal{N}(0, \sigma^2 \text{Id})$ , which is considered in [17], [21], [61]–[63]. The behavior of Poissonian model is fundamentally different from that of AWGN, for which the noise intensity is uniform and independent of the underlying signal.

Our objective is to find an estimate  $\hat{x}$  so that it is the closest possible to  $x$  in the minimum MSE sense. That is, ideally we would like to minimize

$$\text{MSE} = \frac{1}{N} \mathbb{E} \{ \|\hat{x} - x\|^2 \} = \frac{1}{N} \mathbb{E} \left\{ \sum_{n=1}^N (\hat{x}_n - x_n)^2 \right\}, \quad (3)$$

over a set of admissible deconvolution results  $\hat{x}$ . Here  $\mathbb{E}\{\cdot\}$  denotes the mathematical expectation operator.

Instead of iteratively estimating  $\hat{x}$  itself, like current state-of-the-art approaches [23], [29], [37], [38], we choose to express the processing as an explicit function  $\mathbf{F} : \mathbb{R}^N \rightarrow \mathbb{R}^N$  of the measured  $y$  such that  $\hat{x} = \mathbf{F}(y)$ , as shown in Fig. 2. Then the MSE becomes:

$$\text{MSE} = \frac{1}{N} \mathbb{E} \{ \|\mathbf{F}(y) - x\|^2 \}. \quad (4)$$

### B. The MSE-LET Approach

In order to find the restoration function, we approximate it as a *linear* combination of  $K$  *non-linear* elementary functions  $\mathbf{F}_k$  (Fig.3), termed “linear expansion of thresholds” (LET) [2], [21], [56]:

$$\mathbf{F}(y) = \sum_{k=1}^K a_k \mathbf{F}_k(y), \quad (5)$$

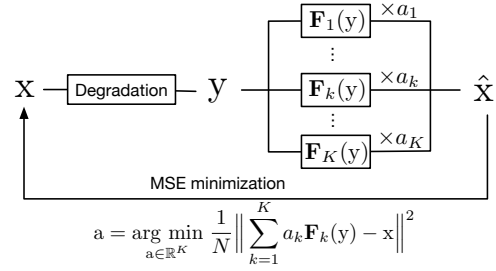


Fig. 4. Principle of the MSE-LET approach. The processing function  $\mathbf{F}$  is described as a linear combination of  $K$  possibly non-linear processing  $\mathbf{F}_k$ . The optimal coefficients  $a_k$  are obtained by minimizing the MSE.

where  $K \ll N$  is the number of linear coefficients  $a = [a_k]_{k \in [1, \dots, K]}$  of the LETs. Accordingly, the deconvolution problem reduces to finding the linear coefficients  $a_k$  by minimizing the MSE, as shown in Fig. 4, and to solving

$$\min_{a_k} \left\| \sum_{l=1}^K a_l \mathbf{F}_l(y) - x \right\|^2,$$

which leads to a linear system of equations:

$$\sum_{l=1}^K \mathbf{F}_k(y) \mathbf{F}_l(y) a_l = \mathbf{F}_k(y)^T x, \quad \forall k \in [1, K].$$

The number of parameters  $K$  used to describe the estimator  $\mathbf{F}(y)$  should remain much lower than the number of observations  $N$  (typically, the number of image pixels) to avoid fitting of the observed data. Note that this LET approach does not imply any hypothesis on the unknown image  $x$  itself, although we may wish to choose the elementary functions  $\mathbf{F}_k$  to span the space of “good” processing (which may build upon the hypothesis that usual images are essentially low-pass). This strategy has proven to be very effective in image denoising [2], [56] and image deconvolution in Gaussian noise [21]. In particular, it comes to be a reasonable idea to use simple deconvolution processes (like Wiener filtering) followed by some forms of wavelet denoising as templates for our LET basis elementary functions.

However, in practice we do not have access to the oracle MSE between  $x$  and the estimate  $\mathbf{F}(y)$  since  $x$  is unknown. Fortunately, it is possible to obtain an unbiased estimate of its expected value (termed as PURE), which solely depends on the observed image  $y$ . Then we just replace the MSE minimization by the minimization of its unbiased estimate PURE to determine the optimal coefficients.

### C. The PURE-LET Approach

In what follows, we will firstly consider the Poisson noise model (2) and then go to the mixed Poisson-Gaussian noise model (1).

1) *Poisson Noise Case*: Considering the linear degradation model (2), the mathematical expectation of the MSE between a given estimate  $\hat{x} = \mathbf{F}(y)$  and  $x$  can be expressed using only the observed image  $y$ . We have the following theorem:

**Theorem 1 (PURE).** *Let  $\mathbf{F}(y) = [f_n(y)]_{n=1 \dots N}$  be an  $N$ -dimensional real-valued vector function. We assume the linear*

degradation model (2) and that  $\mathbf{H}$  is invertible, then the random variable

$$\text{PURE}\{\mathbf{F}\} = \frac{1}{N} \|\mathbf{F}(\mathbf{y})\|^2 - \frac{2}{N} \mathbf{y}^T \mathbf{H}^{-T} \mathbf{F}^-(\mathbf{y}) + \mathcal{E}_{\mathcal{P}}, \quad (6)$$

is an unbiased estimate of the expected MSE; i.e.,

$$\mathbb{E}\{\text{PURE}\} = \frac{1}{N} \mathbb{E} \{ \|\mathbf{F}(\mathbf{y}) - \mathbf{x}\|^2 \},$$

where  $\mathbf{F}^-(\mathbf{y}) \stackrel{\text{def}}{=} [f_n(\mathbf{y} - \alpha \mathbf{e}_n)]_{n=1, \dots, N}$ ,  $\mathbf{e}_n$  is the  $N$ -dimensional vector with components  $\delta_{k-n}$ ,  $k = 1, 2, \dots, N$ ,  $\mathcal{E}_{\mathcal{P}} = (\mathbf{y}^T \mathbf{H}^{-T} \mathbf{H}^{-1} \mathbf{y} - \alpha \mathbf{1}^T \mathbf{H}^{-T} \mathbf{H}^{-1} \mathbf{y}) / N$  is independent on  $\mathbf{F}$ .

The unbiasedness between PURE and MSE and the fact that  $N$  is large indicate that (6) can be used as a reliable substitute of the MSE (law of large numbers: a sample mean like the PURE and the MSE, is close to its mathematical expectation). All terms are computable in practice since we replace the MSE by a statistical equivalent that does not depend on  $\mathbf{x}$  anymore.

2) *Mixed Poisson-Gaussian Noise Case:* For the linear degradation model (1), we derive the unbiased estimate of MSE, SPURE (Stein-Poisson unbiased risk estimate). It is given in the following theorem.

**Theorem 2 (SPURE).** *Under the same hypotheses as Theorem 1, and now assume  $\mathbf{F}(\mathbf{y})$  is boundedly differentiable. Considering the linear degradation model (1) and assuming  $\mathbf{H}$  is invertible, then the random variable*

$$\begin{aligned} \text{SPURE}\{\mathbf{F}\} &= \frac{1}{N} \|\mathbf{F}(\mathbf{y})\|^2 - \frac{2}{N} \mathbf{y}^T \mathbf{H}^{-T} \mathbf{F}^-(\mathbf{y}) \\ &+ \frac{2\sigma^2}{N} \text{div}\{\mathbf{H}^{-T} \mathbf{F}^-(\mathbf{y})\} + \mathcal{E}_{\mathcal{P}+\mathcal{G}}, \end{aligned} \quad (7)$$

is an unbiased estimate of the expected MSE, where  $\mathbf{F}^-(\mathbf{y}) \stackrel{\text{def}}{=} [f_n(\mathbf{y} - \alpha \mathbf{e}_n)]_{n=1, \dots, N}$ ,  $\mathbf{e}_n$  is the  $N$ -dimensional vector with components  $\delta_{k-n}$ ,  $k = 1, 2, \dots, N$ , and  $\text{div}\{\mathbf{F}\} = \sum_n \partial f_n / \partial x_n$  is the divergence of a vector function  $\mathbf{F}$ .  $\mathcal{E}_{\mathcal{P}+\mathcal{G}} = \mathcal{E}_{\mathcal{P}} - \sigma^2 \text{Tr}\{\mathbf{H}^{-T} \mathbf{H}^{-1}\} / N$  is independent on  $\mathbf{F}$ .

The proof of Theorem 2 (which implies Theorem 1) is given in Appendix. The term  $\text{div}\{\mathbf{H}^{-T} \mathbf{F}^-(\mathbf{y})\}$  in (7) corresponds to the contribution of the Gaussian component of the noise, while  $\mathbf{y}^T \mathbf{H}^{-T} \mathbf{F}^-(\mathbf{y})$  is due to the Poisson component, respectively. If the Poisson component of the noise is absent, this unbiased estimate becomes the Stein's unbiased risk estimate (SURE) [21], [64]

$$\begin{aligned} \text{SURE} &= \frac{1}{N} \|\mathbf{F}(\mathbf{y})\|^2 - \frac{2}{N} \mathbf{y}^T \mathbf{H}^{-T} \mathbf{F}(\mathbf{y}) \\ &+ \frac{2\sigma^2}{N} \text{div}\{\mathbf{H}^{-T} \mathbf{F}(\mathbf{y})\} - \frac{\sigma^2}{N} \text{Tr}\{\mathbf{H}^{-T} \mathbf{H}^{-1}\}, \end{aligned}$$

which is the unbiased risk estimate corresponding to a pure additive Gaussian noise model for the deconvolution problem. Note that the SURE was initially employed for the image denoising problem [56], [65]–[68]. We would like to point out that these unbiased estimates, PURE in (6) and SPURE in (7), may also be used in conventional iterative regularization-based deconvolution algorithms (e.g. [29], [34], [37], [38]), to find the optimal regularization parameters or the optimal number

of iterations. The divergence terms can be estimated reliably by a Monte-Carlo technique, see [69] and [44].

### Implementation Notes.

- 1) *Conditioning of the matrix  $\mathbf{H}$ .* If the matrix  $\mathbf{H}$  is ill-conditioned, PURE will fail to be a reliable estimate of the MSE. To keep the stability of the PURE, the Tikhonov-regularized inverse [10], [21] is used to approximate  $\mathbf{H}^{-1}$ :

$$\mathbf{H}_{\beta}^{-1} = (\mathbf{H}^T \mathbf{H} + \beta \mathbf{P}^T \mathbf{P})^{-1} \mathbf{H}^T, \quad (8)$$

for some parameter  $\beta > 0$  and matrix  $\mathbf{P} \in \mathbb{R}^{N \times N}$  for which  $\|\mathbf{P}\mathbf{x}\|$  is known to be small (typically  $\mathbf{P}$  is the discrete Laplacian operator).

- 2) *Approximation of the exact PURE [2].* A direct evaluation of  $\mathbf{y}^T \mathbf{H}_{\beta}^{-T} \mathbf{F}^-(\mathbf{y})$  would require the calculation of  $\mathbf{y}^T \mathbf{H}_{\beta}^{-T} \mathbf{F}$  for  $N$  perturbed versions of the input  $\mathbf{y}$ :  $(\mathbf{y} - \alpha \mathbf{e}_n)$  for  $n = 1, \dots, N$ . Such an evaluation would be computationally unrealistic even with images of reasonable size (e.g.  $256 \times 256$ ). Instead, we use the 1st-order derivative to approximate  $\mathbf{y}^T \mathbf{H}_{\beta}^{-T} \mathbf{F}^-(\mathbf{y})$  given by:

$$\mathbf{y}^T \mathbf{H}_{\beta}^{-T} \mathbf{F}^-(\mathbf{y}) \simeq \mathbf{y}^T \mathbf{H}_{\beta}^{-T} (\mathbf{F}(\mathbf{y}) - \alpha \partial \mathbf{F}(\mathbf{y})), \quad (9)$$

where  $\partial \mathbf{F}(\mathbf{y}) = [\frac{\partial f_n(\mathbf{y})}{\partial y_n}]_{n=1, \dots, N}$  is the  $N \times 1$  vector made of the first derivative of each function  $f_n$  with respect to  $y_n$ .

- 3) *Noise parameters.* We assume the noise parameters  $\alpha$  and  $\sigma$  to be known in this work. Several methods are available to estimate them, for example, [1], [70], [71] and more recently [72], [73].

The value of  $\beta$  in (8) should be selected to achieve a good balance between the approximation accuracy and the stability of PURE. In this work, we set  $\beta = 10^{-5} \alpha y_{\text{mean}}$ , where  $y_{\text{mean}} = \mathbb{E}\{y\}$  is the expected value of  $y$ . In fact, this value is not sensitive to our numerical evaluation. Any value of  $\beta \in [5 \times 10^{-6}, 5 \times 10^{-5}] \alpha y_{\text{mean}}$  yields similar results (differences are less than 0.1 dB). The error between the LHS and RHS in (9) is typically bounded by the second order derivative of the component of  $\mathbf{F}$ . So provided that  $\mathbf{F}(\mathbf{y})$  is smooth enough over intervals of length  $\alpha$ ,  $\mathbf{y}^T \mathbf{H}_{\beta}^{-T} \mathbf{F}^-(\mathbf{y})$  is well approximated by (9).

For the Poisson noise case, the unbiased MSE estimate in (6) is then approximated by

$$\begin{aligned} \text{PURE}_{\text{app}}\{\mathbf{F}\} &= \frac{1}{N} \|\mathbf{F}(\mathbf{y})\|^2 - \frac{2}{N} \mathbf{y}^T \mathbf{H}_{\beta}^{-T} \mathbf{F}(\mathbf{y}) \\ &+ \frac{2\alpha}{N} \mathbf{y}^T \mathbf{H}_{\beta}^{-T} \partial \mathbf{F}(\mathbf{y}) + \mathcal{E}_{\mathcal{P}}. \end{aligned} \quad (10)$$

By substituting (5) into (10) and performing differentiation over  $a_k$ , this PURE-LET minimization is equivalent to solving the following linear system of equations:

$$\sum_{k'=1}^K \mathbf{F}_{k'}(\mathbf{y})^T \mathbf{F}_{k'}(\mathbf{y}) a_{k'} = \underbrace{\mathbf{y}^T \mathbf{H}_{\beta}^{-T} (\mathbf{F}_k(\mathbf{y}) - \alpha \partial \mathbf{F}_k(\mathbf{y}))}_{c_k} \quad (11)$$

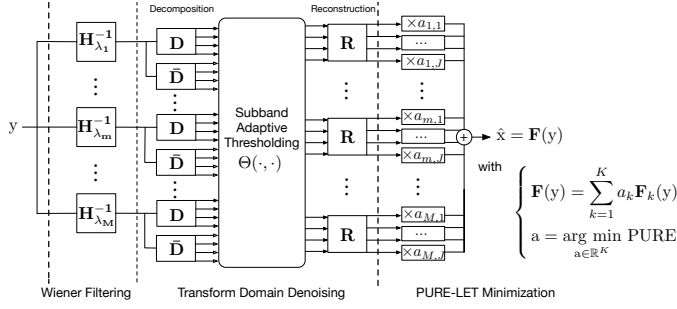


Fig. 5. Principle of the PURE-LET approach. Each elementary function consists of Wiener filtering followed by transform domain denoising. The estimate  $\hat{x}$  is obtained by minimizing (10) or (12). The number of coefficients to be determined is  $K = M \times J \times L$ , where  $M$  is the number of Wiener filters,  $J$  is the number of subbands and  $L$  is the number of thresholding functions. Note that the reconstruction  $\mathbf{R}_j$  performed to the specific  $j$ -th subband only, by setting all the other subbands to zero.

for  $k = 1, 2, \dots, K$ . These equations can be summarized as  $\mathbf{M}\mathbf{a} = \mathbf{c}$ , where  $\mathbf{M} = \mathbf{F}^T \mathbf{F} \in \mathbb{R}^{K \times K}$  and  $\mathbf{c} = [c_1, \dots, c_K]^T \in \mathbb{R}^K$ . We can ensure there will always be a solution to the above linear system since the minimization of  $\text{PURE}_{\text{app}}\{\mathbf{F}\}$  always exists. To cope with the possible singularity of  $\mathbf{M}$ , we solve the following regularized linear system of equations  $\mathbf{a} = (\mathbf{M} + \mu \mathbf{I})^{-1} \mathbf{c}$  where  $\mu = 5 \times 10^{-4} y_{\text{mean}}^2$  is empirically chosen.

As in the Poisson noise case, the  $\text{SPURE}\{\mathbf{F}\}$  in (7) can be approximated by

$$\begin{aligned} \text{SPURE}_{\text{app}} &= \frac{1}{N} \|\mathbf{F}(y)\|^2 - \frac{2}{N} y^T \mathbf{H}_\beta^{-T} (\mathbf{F}(y) - \alpha \partial \mathbf{F}(y)) \\ &+ \frac{2\sigma^2}{N} \text{div} \left\{ \mathbf{H}_\beta^{-T} (\mathbf{F}(y) - \alpha \partial \mathbf{F}(y)) \right\} + \mathcal{E}_{\mathcal{P}+\mathcal{G}}. \end{aligned} \quad (12)$$

In what follows, we keep the name of PURE-LET, even in the mixed Poisson-Gaussian noise case where  $\text{SPURE}$  (12) is minimized. The elementary functions for this mixed Poisson-Gaussian noise case are restricted only by the differentiability assumption of Theorem 2. Similarly, we can obtain a system of  $K$  linear equations as (11) that involves the same matrix  $\mathbf{M}$  and another  $\mathbf{c}$  given by

$$\begin{aligned} c_k &= y^T \mathbf{H}_\beta^{-T} (\mathbf{F}_k(y) - \alpha \partial \mathbf{F}_k(y)) \\ &- \sigma^2 \text{div} \left\{ \mathbf{H}_\beta^{-T} (\mathbf{F}(y) - \alpha \partial \mathbf{F}(y)) \right\} \end{aligned} \quad (13)$$

for  $k = 1, 2, \dots, K$ .

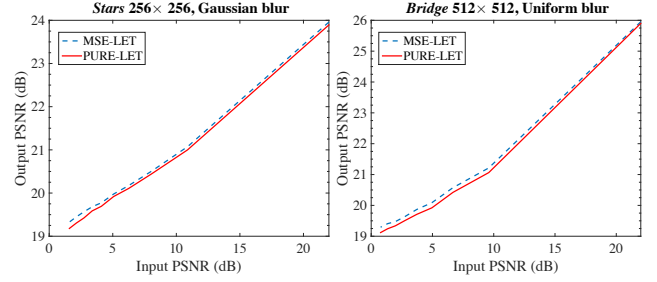
In the next section, we will demonstrate a specific example of the elementary processing  $\mathbf{F}_k$  in the PURE-LET approach for the deconvolution problem of model (1) and (2).

### III. MULTI-WIENER PURE-LET DECONVOLUTION

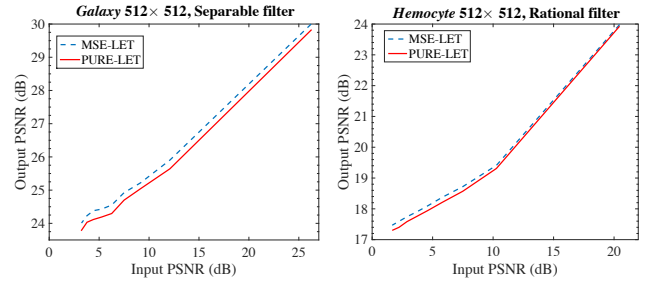
#### A. Construction of Elementary Functions

We choose to construct the elementary functions  $\mathbf{F}_k$ 's as basic deconvolution processes (Wiener filtering) followed by denoising (transform-domain thresholding).

We use an undecimated filterbank transform in this work (typically, Haar wavelet transform), which has proved to be effective for reducing various types of noise degradations [2], [56], [74]. The coefficients provided by the analysis filter are



(a) Poisson noise cases



(b) Mixed Poisson-Gaussian noise cases

Fig. 6. PSNR comparisons of  $\text{MSE-LET}$  and  $\text{PURE-LET}$  for various degradation scenarios where  $\alpha \in [0.1, 500]$ . (a) The Poisson noise cases, where *Stars* and *Bridge* image are blurred by Gaussian kernel and uniform kernel, respectively. (b) The mixed Poisson-Gaussian noise cases, where *Galaxy* image is degraded by separable filter and Poisson noise, and subsequently contaminated by Gaussian noise with  $\sigma = 10$ . *Hemocyte* image is degraded by rational filter and Poisson noise, and subsequently contaminated by Gaussian noise with  $\sigma = 10$ . The maximum difference for all degradation scenarios is 0.265 dB.

thresholded, and then finally passed to the synthesis filter band, as shown in Fig. 5.

The matrices  $\mathbf{H}_{\lambda_k}^{-1} = (\mathbf{H}^T \mathbf{H} + \lambda_k \mathbf{P}^T \mathbf{P})^{-1} \mathbf{H}^T$  represent Wiener filters with a regularization parameter  $\lambda_k$ . Different values of  $\lambda_k$  (typical values: see experiment section) capture different features of the image, thus a suitable combination of  $\mathbf{F}_k$ 's is likely to provide a good balance between noise reduction and edge preservation.  $\mathbf{D} = [d_{i,j}]_{(i,j) \in [1, \dots, L] \times [1, \dots, N]}$  and  $\mathbf{R} = [r_{i,j}]_{(i,j) \in [1, \dots, L] \times [1, \dots, N]}$  represent a pair of linear decomposition and reconstruction filterbanks that satisfy the perfect reconstruction condition  $\mathbf{R}\mathbf{D} = \mathbf{I}$ . A linear transformation (typically, a smoothing)  $\tilde{\mathbf{D}} = [\tilde{d}_{i,j}]_{(i,j) \in [1, \dots, L] \times [1, \dots, N]}$  is applied to the filtered image  $\mathbf{H}_\lambda^{-1} y$  in order to provide a coarse estimation of the transform-domain signal-dependent local noise variance [2]. The deconvolved estimate  $\hat{x}$  can be finally expressed as a function  $\mathbf{F}$  of the blurred noisy input image  $y$  as

$$\hat{x} = \mathbf{F}(y) = \mathbf{R}\Theta \left( \underbrace{\mathbf{D}\mathbf{H}_\lambda^{-1} y}_{\mathbf{w}}, \underbrace{\tilde{\mathbf{D}}\mathbf{H}_\lambda^{-1} y}_{\tilde{\mathbf{w}}} \right), \quad (14)$$

where  $\Theta(\mathbf{w}, \tilde{\mathbf{w}}) = [\theta_l(w_l, \tilde{w}_l)]_{l \in [1, \dots, L]}$  represents the subband-adaptive pointwise (nonlinear) thresholding function. In this work, the  $\tilde{w}_l$  are simply the scaling coefficients of the lowpass residual at a given scale  $l$ .

We further assume that the transform-domain pointwise thresholding function of (14) is continuously differentiable, with piecewise-differentiable partial derivatives. Then for the Poisson noise case, we have the following corollary.

**Corollary 1.** *Given the transform-domain pointwise processing  $\mathbf{F}(\cdot)$  defined by (14), the approximation of the PURE estimate introduced in (10), can be further expressed as*

$$\begin{aligned} \text{PURE}_{\text{app}} &= \frac{1}{N} \|\mathbf{F}(y)\|^2 - \frac{2}{N} y^T \mathbf{H}_\beta^{-T} \mathbf{F}(y) \\ &+ \frac{2\alpha}{N} \left( \partial_w \Theta(w, \bar{w})^T [(\mathbf{D}\mathbf{H}_\lambda^{-1}) \circ (\mathbf{H}_\beta^{-T} \mathbf{R})^T] y + \right. \\ &\quad \left. \partial_{\bar{w}} \Theta(w, \bar{w})^T [(\bar{\mathbf{D}}\mathbf{H}_\lambda^{-1}) \circ (\mathbf{H}_\beta^{-T} \mathbf{R})^T] y \right) + \mathcal{E}_P, \end{aligned}$$

where  $\partial_w \Theta(w, \bar{w})$  and  $\partial_{\bar{w}} \Theta(w, \bar{w})$  represents the first derivative with respect to  $w$  and  $\bar{w}$  of each thresholding function  $\theta_l$ , respectively. “ $\circ$ ” denotes the Hadamard product between two matrices.

The computation of transform-dependent terms can be performed similarly as in the case of Gaussian noise [21]. A similar result for the mixed Poisson-Gaussian noise case is provided by the following corollary.

**Corollary 2.** *Given the transform-domain pointwise processing  $\mathbf{F}(\cdot)$  defined by (14), the approximation of the PURE estimate introduced in (12), can be further expressed as*

$$\begin{aligned} \text{SPURE}_{\text{app}} &= \frac{1}{N} \|\mathbf{F}(y)\|^2 - \frac{2}{N} y^T \mathbf{H}_\beta^{-T} \mathbf{F}(y) \\ &+ \frac{2\alpha}{N} \left( \partial_w \Theta(w, \bar{w})^T [(\mathbf{D}\mathbf{H}_\lambda^{-1}) \circ (\mathbf{H}_\beta^{-T} \mathbf{R})^T] y + \right. \\ &\quad \left. \partial_{\bar{w}} \Theta(w, \bar{w})^T [(\bar{\mathbf{D}}\mathbf{H}_\lambda^{-1}) \circ (\mathbf{H}_\beta^{-T} \mathbf{R})^T] y \right) \\ &+ \frac{2\sigma^2}{N} \left( \text{diag} \left\{ \mathbf{D}\mathbf{H}_\lambda^{-1} \mathbf{H}_\beta^{-T} \mathbf{R} \right\} \partial_w \Theta(w, \bar{w})^T + \right. \\ &\quad \left. \text{diag} \left\{ \bar{\mathbf{D}}\mathbf{H}_\lambda^{-1} \mathbf{H}_\beta^{-T} \mathbf{R} \right\} \partial_{\bar{w}} \Theta(w, \bar{w})^T \right) \\ &- \frac{2\sigma^2}{N} \left( \text{diag} \left\{ (\mathbf{D}\mathbf{H}_\lambda^{-1})^2 (\mathbf{H}_\beta^{-T} \mathbf{R}) \right\} \partial_w^2 \Theta(w, \bar{w})^T + \right. \\ &\quad \left. 2 \text{diag} \left\{ (\mathbf{D}\mathbf{H}_\lambda^{-1}) \circ (\bar{\mathbf{D}}\mathbf{H}_\lambda^{-1}) \mathbf{H}_\beta^{-T} \mathbf{R} \right\} \partial_{w, \bar{w}} \Theta(w, \bar{w})^T + \right. \\ &\quad \left. \text{diag} \left\{ (\bar{\mathbf{D}}\mathbf{H}_\lambda^{-1})^2 \mathbf{H}_\beta^{-T} \mathbf{R} \right\} \partial_{\bar{w}}^2 \Theta(w, \bar{w})^T \right) + \mathcal{E}_{P+G}, \end{aligned}$$

where  $\partial_w \Theta(w, \bar{w}) \in \mathbb{R}^L$  and  $\partial_{\bar{w}} \Theta(w, \bar{w}) \in \mathbb{R}^L$  represents the first derivative with respect to  $w$  and  $\bar{w}$  of each thresholding function  $\theta_l$ , respectively.  $\partial_w^2 \Theta(w, \bar{w}) \in \mathbb{R}^L$  and  $\partial_{\bar{w}}^2 \Theta(w, \bar{w}) \in \mathbb{R}^L$  is the second derivative with respect to  $w$  and  $\bar{w}$  of  $\theta_l$ , respectively.  $\partial_{w, \bar{w}} \Theta(w, \bar{w}) \in \mathbb{R}^L$  is made of the first derivative with respect to  $w$  and  $\bar{w}$  of each function  $\theta_l$ .  $(\mathbf{D}\mathbf{H}_\lambda^{-1})^2$  (resp.  $(\bar{\mathbf{D}}\mathbf{H}_\lambda^{-1})^2$ ) stands for  $(\mathbf{D}\mathbf{H}_\lambda^{-1}) \circ (\mathbf{D}\mathbf{H}_\lambda^{-1})$  (resp.  $(\bar{\mathbf{D}}\mathbf{H}_\lambda^{-1}) \circ (\bar{\mathbf{D}}\mathbf{H}_\lambda^{-1})$ ).

The proofs of Corollary 1 and 2 are similar to that of Corollary 1 in [2]. The whole deconvolution process can be expressed as the following linear combination:

$$\begin{aligned} \mathbf{F}(y) &= \sum_{m=1}^M \sum_{l=1}^L \sum_{j=1}^J a_{m,l,j} \underbrace{\mathbf{R}_j \theta_l(w_{m,j}, \bar{w}_{m,j})}_{\mathbf{F}_{m,j,k}(y)} \\ &\quad + \sum_{m=1}^M \underbrace{\mathbf{R}_{J+1} \mathbf{D}_{J+1} \mathbf{H}_{\lambda_m}^{-1} y}_{\text{lowpass subband}}, \end{aligned}$$

where  $M$  is the number of Wiener filters (typically  $M = 3$ ),  $L$  is the number of elementary pointwise thresholding functions

( $L = 2$  yields satisfactory results), the decomposition and reconstruction matrices are made of  $J(N \times N)$  circulant submatrices  $\mathbf{D}_j$  and  $\mathbf{R}_j$  respectively, and  $J$  denotes the number of highpass wavelet subbands (typically  $J = 12$  for four decomposition levels). Note that as is customary in wavelet-domain thresholding for signal denoising, the  $(J+1)$ th bands, lowpass subbands, are unprocessed. This is supported by experiments that show that the optimal weights for these subbands are almost identical to 1.

## B. Choice of Thresholding Functions

We extend the thresholding functions in [21]

$$\theta(w, T) = w(1 - e^{-(w/T)^4})$$

by taking into account the non-stationarity of the noise, and the following *subband-adaptive* thresholding function  $\theta_{j,l}$  is proposed:

$$\begin{cases} \theta_{j,1}(w, \bar{w}) = \theta(w, 3t_j(\bar{w})) \\ \theta_{j,2}(w, \bar{w}) = \theta(w, 8t_j(\bar{w})), \end{cases} \quad (15)$$

where  $t_j(\bar{w}) = \sqrt{2^{-j} \cdot \tanh(\alpha k \bar{w}) \alpha \bar{w} + \sigma^2}$  and  $k$  is empirically set to 100, so that  $t_j(\bar{w}) \simeq \sqrt{2^{-j} |\alpha \bar{w}| + \sigma^2}$ . Note that each transformed coefficient is adaptively thresholded according to its estimated amount of noise, thanks to these signal-dependent thresholding functions. Linear combinations of these two thresholding functions approximate intermediate thresholds of the form  $\theta(w, T)$  for  $T/t_j(\bar{w}) \in [3, 8]$ , a range that has been optimized empirically.

As indicated by (11), there are  $K = M \times J \times L$  parameters to be determined and they are given by the solution of the linear system of equations (11) of order  $K$ .

## IV. EXPERIMENTS AND RESULTS

### A. Experimental Setting

All experiments are carried out on a Macbook Pro with a 2.4 GHz Intel Core i5, with 8 GB of RAM. The original images are firstly convolved by different blur kernels, and subsequently contaminated by Poisson noise or mixed Poisson-Gaussian noise. The noise levels correspond to different  $\alpha$  in the Poisson noise case, and both  $\alpha$  and  $\sigma^2$  in the mixed Poisson-Gaussian noise case. The algorithm performance is measured by the peak signal-to-noise ratio (PSNR), defined as  $\text{PSNR} = 10 \log_{10}(I_{\text{max}}^2 / (\|\hat{x} - x\|^2 / N))$ , where  $I_{\text{max}}$  is the maximum intensity of the noise-free image.

In the proposed method, we use  $M = 3$  Wiener filters with  $\lambda_1 = 10^{-4} \alpha y_{\text{mean}}$ ,  $\lambda_2 = 10^{-3} \alpha y_{\text{mean}}$  and  $\lambda_3 = 10^{-2} \alpha y_{\text{mean}}$ , where  $y_{\text{mean}}$  is the expected value of  $y$ . The undecimated Haar wavelet transform is used because of its substantial outperformance over other types of redundant wavelets in image denoising [2], [56]. This observation also holds for image deconvolution [21]. The decomposition level is set to be 4 ( $J = 12$ ). Thus we will have  $K = 3 \times 2 \times 12 = 72$  coefficients to be determined via solving (11) or (13).

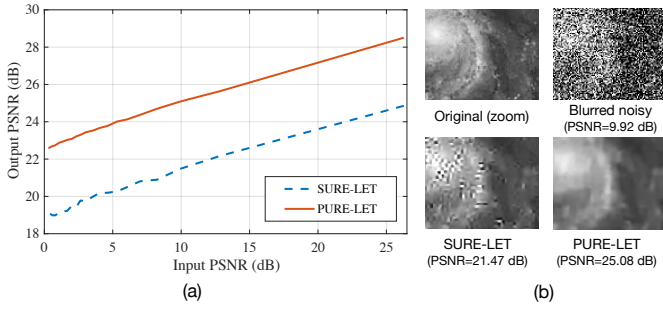


Fig. 7. An algorithm designed for additive Gaussian noise is significantly sub-optimal for Poisson noise corrupted data: (a) PSNR comparisons of SURE-LET [21] and PURE-LET for *Galaxy* image (Fig. 8(c)) degraded by Gaussian blur (variance is 3) with Poisson noise  $\alpha \in [1, 1000]$ ; (b) One typical example when  $\alpha = 100$ .

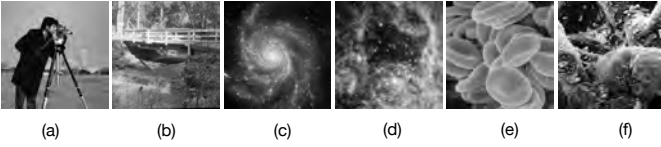


Fig. 8. Set of original natural images. (a) *Cameraman*  $256 \times 256$ ; (b) *Bridge*  $512 \times 512$ ; (c) *Galaxy*  $256 \times 256$ ; (d) *Stars*  $256 \times 256$ ; (e) *Erythrocyte*  $512 \times 512$ ; (f) *Hemocyte*  $512 \times 512$ .

## B. Validation

1) *PURE-LET vs MSE-LET*: To validate the use of the PURE and its associated approximations as an accurate prediction of the MSE, we compare the performance of PURE-LET approach to the optimal performance achieved when using the MSE minimization in the LET framework. In other words, the MSE is used directly in (11) leading to an oracle solution obtained by the pointwise thresholding proposed in (15) and solving  $\mathbf{M}\mathbf{a}_{\text{MSE}} = \mathbf{F}^T \mathbf{x}$ . The comparison of PURE-LET and *MSE-LET* for four typical degradation scenarios is shown in Fig. 6. In the Poisson noise cases, the maximum difference between the oracle *MSE-LET* and the proposed PURE-LET is 0.148 dB and 0.173 dB respectively. In the mixed Poisson-Gaussian noise cases, their maximum difference is 0.265 dB and 0.194 dB, respectively. As expected, our PURE-LET consistently remains within 0.3 dB from the *MSE-LET* for a wide range of noise levels and different kernels, which is an evidence that the approximated PURE is an accurate predictor of the MSE.

2) *Poisson vs Gaussian deconvolution algorithms*: We also compare PURE-LET with SURE-LET deconvolution algorithm [21]. SURE-LET is one of the state-of-the-art methods designed for Gaussian noise removal. The noise variance needed by SURE-LET is estimated by the mean squared error between the blurred noisy image and the blurred image. Fig. 7 shows PSNRs under different noise levels (different values of  $\alpha$ ), and visual comparisons for *Galaxy* image (see Fig. 8(c)). It can be seen that PURE-LET outperforms SURE-LET in these scenarios, and the differences are significant (maximum difference is 4.68 dB). This comparison demonstrates the distinct advantage of considering the Poisson noise statistics: Gaussian-noise based restoration algorithms are significantly sub-optimal.

## C. Poisson Noise Case

We perform experiments over six images, which consist of two natural images<sup>1</sup> of size  $256 \times 256$  (*Cameraman*) and of size  $512 \times 512$  (*Bridge*), two astronomical images<sup>2</sup> of size  $256 \times 256$  (*Galaxy*, *Stars*) and two biological images<sup>3</sup> of size  $512 \times 512$  (*Erythrocyte*, *Hemocyte*). They were converted to grayscale and displayed in Fig. 8.

The performance of each method is assessed for various convolution kernels and different noise levels. In particular, we consider the following five benchmark convolution kernels:

- 1) Gaussian blur with variance 3;
- 2)  $5 \times 5$  uniform blur;
- 3) Separable filter:  $5 \times 5$  filter with weights  $[1, 4, 6, 4, 1]/16$  along both horizontal and vertical directions;
- 4) Rational filter:  $h(i, j) = (1 + i^2 + j^2)^{-1}$  for  $i, j = -7, \dots, 7$ ;

Each image is further corrupted with Poisson noise at six different noise levels  $\alpha \in [2, 4, 8, 32, 128, 256]$ . The input PSNR for each noise level, for all images, varies in the range of  $[19.95, 25.70]$ ,  $[18.73, 23.29]$ ,  $[16.57, 20.67]$ ,  $[10.73, 14.94]$ ,  $[4.76, 8.97]$ ,  $[1.74, 5.97]$  covering a wide gamut of noise levels. Note that we have averaged the output PSNRs over ten noise realizations and different methods are applied to the same noise realization.

As benchmarks for comparisons, we evaluate our method against five state-of-the-art deconvolution techniques specifically designed for Poisson noisy images: *PoissonDeconv*<sup>4</sup> [38], *PIDAL* [22], *SPIRAL-TAP-TI*<sup>5</sup> [29], *PoissonHessReg*<sup>6</sup> [23] and *GILAM*<sup>7</sup> [37]. The source code of *PIDAL* is kindly included in the *GILAM* package. For each of these methods, we used the parameters suggested in their respective publications and softwares.

Table I reports the PSNR results we have obtained from the various deconvolution methods under Gaussian blur with variance 3, the best results within a 0.1 dB margin are shown in boldface. Table II reports the PSNR results of the *Hemocyte* image for various blurs and noise levels. It is clear that, the PURE-LET approach consistently outperforms other approaches often by a significant margin. We would also like to stress that our algorithm is very robust to a wide range of noise levels. In particular, significant improvements are observed at large  $\alpha$ , where the signal-dependent nature of the Poisson noise is more pronounced. Fig. 9 and Fig. 10 show the comparison of visual quality of *Bridge* and *Hemocyte*, respectively. We observe that our method preserves various image details, while introducing very few artifacts.

Table III reports the computational time of various deconvolution algorithms. It can be seen that our method is sub-

<sup>1</sup>Natural images are available at <http://decsai.ugr.es/cvg>.

<sup>2</sup>Astronomical images are available at <http://www.hubblesite.org>.

<sup>3</sup>Biological images are available at <http://www.cellimagelibrary.org>.

<sup>4</sup>The source code of *PoissonDeconv* is available at <http://fxdupe.free.fr/software.html>.

<sup>5</sup>The source code of *SPIRAL-TAP-TI* is available at <http://drz.ac/code/spiraltap/>.

<sup>6</sup>The source code of *PoissonHessReg* is available at <http://www.math.ucla.edu/~stamatis/software/PoissonHessReg.zip>.

<sup>7</sup>The source code of *GILAM* is available at [https://www.researchgate.net/profile/Daiqiang\\_Chen\\_chendaiqiang](https://www.researchgate.net/profile/Daiqiang_Chen_chendaiqiang).

TABLE I

PSNR COMPARISON WITH SOME STATE-OF-THE-ART ALGORITHMS UNDER GAUSSIAN BLUR WITH VARIANCE 3. RESULTS HAVE BEEN AVERAGED OVER 10 NOISE REALIZATIONS.

$\alpha$	2	4	8	32	128	256	2	4	8	32	128	256
Image	<i>Cameraman</i> $256 \times 256$						<i>Bridge</i> $512 \times 512$					
Input	20.56	19.02	16.98	11.88	6.11	3.16	20.90	19.34	17.29	12.17	6.41	3.44
PoissonDeconv	22.61	22.28	21.84	19.97	13.58	10.08	22.65	22.36	21.93	19.91	13.67	10.53
PIDAL	23.51	22.89	22.18	20.25	18.32	17.73	23.21	22.52	21.73	19.89	18.37	17.85
SPIRAL-TAP-TI	23.83	23.33	22.54	21.05	19.34	19.32	22.52	21.87	21.50	20.84	17.62	14.46
PoissonHessReg	22.65	22.15	21.57	20.19	18.28	17.25	22.60	22.09	21.52	20.19	18.75	18.02
GILAM	23.80	22.87	21.66	18.56	16.70	15.71	23.28	22.17	20.80	18.39	16.83	16.37
PURE-LET	<b>24.04</b>	<b>23.63</b>	<b>23.13</b>	<b>21.88</b>	<b>20.49</b>	<b>19.72</b>	<b>23.53</b>	<b>23.09</b>	<b>22.64</b>	<b>21.58</b>	<b>20.40</b>	<b>19.70</b>
Image	<i>Galaxy</i> $256 \times 256$						<i>Stars</i> $256 \times 256$					
Input	24.76	22.77	20.34	14.83	8.95	5.95	21.00	19.59	17.68	12.71	6.99	4.04
PoissonDeconv	27.27	26.68	25.96	23.36	16.64	13.91	22.35	22.01	21.60	19.67	14.09	11.27
PIDAL	<b>28.03</b>	27.38	26.64	25.00	23.38	22.65	22.82	22.29	21.64	19.94	18.40	17.90
SPIRAL-TAP-TI	27.43	27.03	26.83	25.72	22.20	21.89	21.91	21.48	21.12	20.77	19.72	17.55
PoissonHessReg	27.63	27.12	26.55	25.44	24.05	23.39	22.51	22.10	21.65	20.48	19.16	18.58
GILAM	27.88	26.97	25.81	23.45	20.90	19.22	22.78	21.92	20.77	18.53	17.29	16.72
PURE-LET	<b>28.11</b>	<b>27.74</b>	<b>27.22</b>	<b>26.21</b>	<b>24.99</b>	<b>24.24</b>	<b>22.97</b>	<b>22.62</b>	<b>22.27</b>	<b>21.35</b>	<b>20.35</b>	<b>19.66</b>
Image	<i>Erythrocyte</i> $512 \times 512$						<i>Hemocyte</i> $512 \times 512$					
Input	22.27	19.52	16.66	10.75	4.75	1.74	20.88	19.59	17.79	12.96	7.30	4.35
PoissonDeconv	29.27	28.16	26.77	22.42	12.60	8.98	21.63	22.08	21.11	18.98	14.10	11.28
PIDAL	<b>31.13</b>	29.68	27.97	24.06	21.15	20.23	23.17	22.11	20.94	18.41	16.36	15.65
SPIRAL-TAP-TI	28.30	26.77	25.86	23.99	14.20	8.55	22.90	22.81	21.66	18.53	16.65	17.21
PoissonHessReg	30.68	29.64	28.40	25.33	21.73	20.30	22.17	21.40	20.53	18.73	16.96	16.21
GILAM	30.02	27.80	25.14	20.88	18.48	17.72	23.33	21.87	20.06	16.69	14.56	13.79
PURE-LET	<b>31.15</b>	<b>30.10</b>	<b>29.11</b>	<b>26.89</b>	<b>24.31</b>	<b>22.89</b>	<b>23.76</b>	<b>23.16</b>	<b>22.48</b>	<b>20.93</b>	<b>19.26</b>	<b>18.42</b>

\* Best PSNR results within a 0.1 dB margin are highlighted.



Fig. 9. Restoration of the *Bridge* image degraded by Gaussian blur with variance 3 and Poisson noise level  $\alpha = 8$ .

stantially faster than other iterative approaches. As observed, the proposed PURE-LET algorithm is roughly 7 times faster than the next fastest algorithm for a  $256 \times 256$  image and 5 times faster for a  $512 \times 512$  image. It is worth mentioning that our method is implemented using unoptimized MATLAB code only, without any compiled routines. In addition, the proposed approach is by nature highly parallelizable for even faster

processing because each basis function  $\mathbf{F}_k$  can be processed independently of the others.

#### D. Mixed Poisson-Gaussian Noise Case

To the best of our knowledge, there are very few deconvolution algorithms that are designed for the mixed Poisson-Gaussian noise case, even though this noise model is more

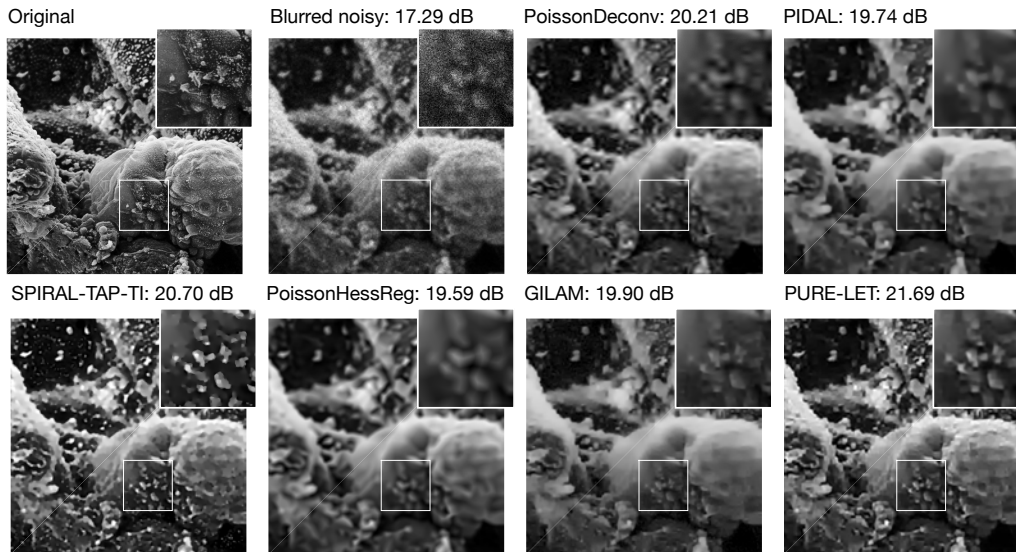


Fig. 10. Restoration of the *Hemocyte* image degraded by Rational filter and Poisson noise level  $\alpha = 8$ .

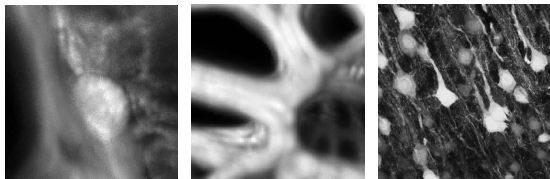


Fig. 11. Set of original images. From left to right: *Image 1*  $190 \times 190$ , *Image 2*  $128 \times 128$ , and *Image 3*  $256 \times 256$ .

realistic. We compare the proposed approach with the method in [48]. Since their method needs to carefully select the regularization parameters for each scenario, we follow their experiment settings in their provided code<sup>8</sup>. Specifically, the considered ground truth image set, including *Image 1* of size  $190 \times 190$ , *Image 2* of size  $128 \times 128$  and *Image 3* of size  $256 \times 256$ , are shown in Fig. 11. The parameters for these degradation scenarios are listed in Tab. IV. We choose the exact model with Hessian-TV prior since it leads to the best qualitative results compared with other models.

Table V reports the comparison results we have obtained from the method in [48] and our method, in terms of PSNR and computational time. Fig. 12 shows a visual comparison. It can be seen the proposed PURE-LET algorithm significantly achieves better performance than [48] both in restoration quality and computational time. In particular, our approach exhibits very few artifacts and is able to retrieve more image details, contrary to the method in [48].

## V. APPLICATION TO REAL FLUORESCENCE MICROSCOPY IMAGES

We now apply the PURE-LET algorithm to the restoration of real 2D confocal fluorescence microscopy images. Although 3D deconvolution is often preferable in wide-field microscopy [10], [75], it is meaningful to apply 2D deconvolution to thin specimen [76], [77]. The dataset we used is the image of

<sup>8</sup>The source code is available at <http://www.ibspan.waw.pl/~jeziersk/software.html>.

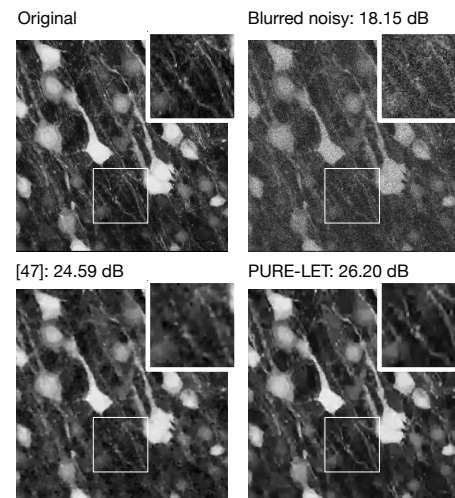


Fig. 12. Restoration of *Image 3*. The computational time of PURE-LET is 1.36 s while [48] needs 1570.40 s.

Exocyst-positive organelles (EXPOs) labeled by AtExo70E2-GFP in Arabidopsis suspension cells [78], acquired on a Leica TCS SP8 confocal laser scanning microscope with a 63x/1.2 water-immersion objective at the School of Life Science of the Chinese University of Hong Kong. Images are of size  $512 \times 512$ , and the pixel dimension is  $0.92 \times 0.92 \mu\text{m}$ .

The optical sectioning ability of a confocal microscope is a function of the pinhole size. A larger pinhole size leads to more out-of-focus light detected, resulting in lower resolution. With a fully open pinhole, the confocal microscope is close to a conventional wide-field microscope. By changing the pinhole size of the confocal microscope, we can balance the optical resolution and light intensity (Fig. 13). A pinhole of 1 airy unit (AU) typically gives the best signal-to-noise ratio, thus provides a pseudo ground truth for evaluation of the deconvolution performance.

We applied our deconvolution algorithm on images collected

TABLE II  
PSNR COMPARISON WITH SOME STATE-OF-THE-ART ALGORITHMS OF THE *Stars* IMAGE AND THE *Hemocyte* IMAGE FOR VARIOUS BLURS AND NOISE LEVELS. RESULTS HAVE BEEN AVERAGED OVER 10 NOISE REALIZATIONS.

Image	<i>Stars</i> 256 × 256						<i>Hemocyte</i> 512 × 512					
	2	4	8	32	128	256	2	4	8	32	128	256
Blur	Uniform blur						Uniform blur					
Input	20.97	19.57	17.67	12.68	6.98	4.04	21.10	19.76	17.90	13.00	7.31	4.36
PoissonDeconv	22.49	22.13	21.59	19.70	13.98	10.50	22.39	22.25	21.34	19.00	14.13	10.82
PIDAL	<b>23.10</b>	22.55	21.85	20.04	18.43	17.92	23.83	22.73	21.46	18.63	16.40	15.68
SPIRAL-TAP-TI	22.65	19.85	17.24	15.01	15.09	15.89	23.32	23.34	<b>22.77</b>	21.09	19.12	18.08
PoissonHessReg	22.72	22.29	21.79	20.57	19.19	18.59	22.70	21.85	20.90	18.91	17.02	16.24
GILAM	22.98	22.05	20.82	18.54	17.29	16.72	23.72	22.18	20.23	16.71	14.55	13.79
PURE-LET	<b>23.17</b>	<b>22.83</b>	<b>22.43</b>	<b>21.45</b>	<b>20.40</b>	<b>19.63</b>	<b>24.15</b>	<b>23.55</b>	<b>22.86</b>	<b>21.20</b>	<b>19.21</b>	<b>18.30</b>
Blur	Separable filter						Separable filter					
Input	22.00	20.28	18.10	12.84	7.02	4.05	22.73	20.89	18.60	13.21	7.37	4.39
PoissonDeconv	22.91	22.44	21.87	19.82	12.46	10.25	23.33	22.81	22.62	19.47	13.04	10.54
PIDAL	<b>23.90</b>	23.19	22.31	20.18	18.45	17.92	<b>25.46</b>	24.19	22.62	19.05	16.47	15.70
SPIRAL-TAP-TI	23.51	21.81	19.96	17.54	14.40	13.26	25.20	24.60	23.70	21.73	18.70	16.36
PoissonHessReg	23.20	22.64	22.04	20.68	19.24	18.62	24.03	22.87	21.62	19.19	17.11	16.30
GILAM	23.49	22.30	20.87	18.54	17.30	16.72	24.73	22.78	20.49	16.72	14.55	13.79
PURE-LET	<b>23.87</b>	<b>23.40</b>	<b>22.89</b>	<b>21.75</b>	<b>20.44</b>	<b>19.76</b>	<b>25.48</b>	<b>24.75</b>	<b>23.90</b>	<b>21.94</b>	<b>19.72</b>	<b>18.56</b>
Image	Rational filter						Rational filter					
Input	20.71	19.37	17.54	12.66	6.97	4.02	19.94	18.87	17.29	12.79	7.26	4.33
PoissonDeconv	21.69	21.33	20.93	18.43	14.04	11.15	20.85	20.28	20.21	18.03	13.90	11.21
PIDAL	22.28	21.70	21.07	19.66	18.31	17.86	22.02	20.81	19.74	17.79	16.18	15.57
SPIRAL-TAP-TI	21.91	19.82	17.79	12.50	10.57	11.95	21.82	21.74	20.70	17.66	16.73	16.96
PoissonHessReg	21.97	21.61	21.21	20.20	19.02	18.44	20.95	20.28	19.59	18.20	16.70	16.07
GILAM	<b>22.63</b>	21.83	20.76	18.55	17.29	16.72	23.07	21.62	19.90	16.69	14.55	13.79
PURE-LET	<b>22.65</b>	<b>22.25</b>	<b>21.86</b>	<b>21.01</b>	<b>20.04</b>	<b>19.46</b>	<b>23.29</b>	<b>22.50</b>	<b>21.69</b>	<b>20.15</b>	<b>18.67</b>	<b>17.97</b>

\* Best PSNR results within a 0.1 dB margin are highlighted.

TABLE III  
COMPARISON OF THE COMPUTATIONAL TIME OF VARIOUS DECONVOLUTION ALGORITHMS (UNITS: SECONDS).

Degradation scenario	PoissonDeconv	PIDAL	SPIRAL-TAP-TI	PoissonHessReg	GILAM	PURE-LET
<i>Cameraman</i> 256 × 256 Gaussian blur, $\alpha = 2$	281.43	9.38	68.31	20.23	12.48	<b>1.31</b>
<i>Galaxy</i> 256 × 256 Uniform blur, $\alpha = 4$	262.93	9.41	8.47	20.01	16.64	<b>1.29</b>
<i>Erythrocyte</i> 512 × 512 Separable filter, $\alpha = 32$	1053.25	41.45	40.92	115.82	39.06	<b>6.45</b>
<i>Hemocyte</i> 512 × 512 Rational filter, $\alpha = 256$	1033.50	68.49	31.37	113.29	67.84	<b>6.30</b>

TABLE IV  
DEGRADATION PARAMETERS OF ALL IMAGES IN THE MIXED  
POISSON-GAUSSIAN NOISE CASE

Image	Gaussian blur $h$	Poisson noise $\alpha$	Gaussian noise $\sigma^2$
Image 1	size = 25 × 25, std = 1.6	21.25	9
Image 2	size = 25 × 25, std = 1.6	8.5	12
Image 3	size = 9 × 9, std = 0.5	4.25	36

TABLE V  
COMPARISON WITH [48] IN TERMS OF PSNR AND COMPUTATIONAL TIME

Method	PSNR (dB)			Computational time (sec)	
	Input	[48]	PURE-LET	[48]	PURE-LET
Image 1	10.33	28.00	<b>29.24</b>	403.10	<b>0.80</b>
Image 2	15.15	26.67	<b>27.05</b>	911.72	<b>0.43</b>
Image 3	18.15	24.59	<b>26.20</b>	1570.40	<b>1.36</b>

in the condition of pinhole size equal to 3AU. The optical PSF of the confocal fluorescence microscope is modeled using the 2D Gaussian kernel [79], parametrized by its variance, whose value is estimated empirically. In order for these images to fit the degradation model described in (1) and find the two parameters  $\sigma^2$  and  $\alpha$ , we use a robust linear regression performed on a collection of local estimates of the sample mean and sample variance, similar to [2], [80].

Fig. 14 shows the results obtained with the PURE-LET deconvolution algorithm for three images with pinhole size 3AU. It can be observed that the restored images are very close to the pseudo ground truth, whose contrast and resolution are improved. Note that compared with the images with pinhole size 3AU, the difference is not just the sharpness of these images, but also the ability of resolving the internal structures. The EXPO dots in the restored images can be distinguished

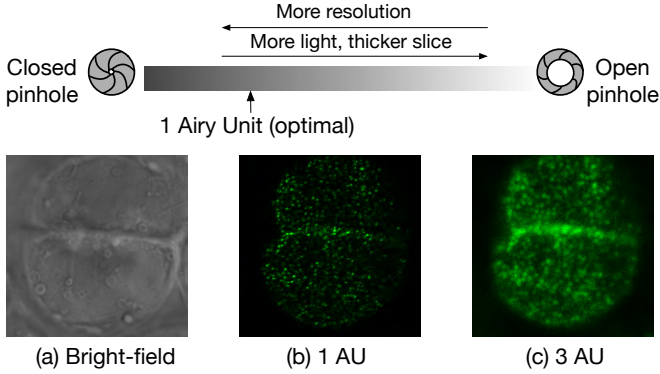


Fig. 13. Illustration of the effect of changing the pinhole size in the confocal microscope.

clearly. Moreover, compared with the images with pinhole size 1AU, the noise caused by the low light condition is reduced as well. We suspect these results could be further improved using a more realistic PSF model [10], [81].

## VI. CONCLUSION

We propose a new non-iterative deconvolution approach for blurred and noisy images with Poisson noise or mixed Poisson-Gaussian noise. We linearly parametrize the deconvolution process as a linear combination of elementary functions (LET). Each elementary function consists of a Wiener filtering followed by transform-domain thresholding. We then use the data-driven unbiased estimate of the MSE (PURE) to optimize the coefficients of this linear combination. The proposed PURE-LET approach outperforms state-of-the-art techniques, both qualitatively and computationally. We then apply it to real confocal fluorescence microscopy images to demonstrate its potential on improving their resolutions. The flexibility and low computational cost of the proposed approach offer a framework for developing more sophisticated algorithms. For example, other transforms such as the block discrete cosine transform and the combination with the discrete wavelet transform, could be employed. We are currently extending this PURE-LET framework to 3D deconvolution: the preliminary results [16] on wide-field fluorescence microscopy images are very promising.

### APPENDIX A PROOF OF THEOREM 2

The data are modeled according to

$$y = p + g,$$

where  $p \sim \alpha\mathcal{P}(\mathbf{H}\mathbf{x}/\alpha)$  and  $g \sim \mathcal{N}(0, \sigma^2\text{Id})$  are  $N$ -dimensional vector random variables. By expanding the expectation of the MSE between  $\mathbf{x}$  and its estimate  $\mathbf{F}(y)$ , we get (note that  $\mathbf{x}$  is not random):

$$\begin{aligned} \mathbb{E} \{ \|\mathbf{F}(y) - \mathbf{x}\|^2 \} &= \mathbb{E} \{ \|\mathbf{F}(y) - \mathbf{x}\|^2 \} \\ &= \mathbb{E} \{ \|\mathbf{F}(y)\|^2 \} - 2\mathbb{E} \{ \mathbf{x}^T \mathbf{F}(y) \} + \|\mathbf{x}\|^2 \\ &= \mathbb{E} \{ \|\mathbf{F}(y)\|^2 \} - 2\mathbb{E} \{ (\mathbf{H}\mathbf{x})^T \mathbf{H}^{-T} \mathbf{F}(y) \} \\ &\quad + \mathbb{E} \{ (\mathbf{H}\mathbf{x})^T \mathbf{H}^{-T} \mathbf{H}^{-1} y \}. \end{aligned}$$

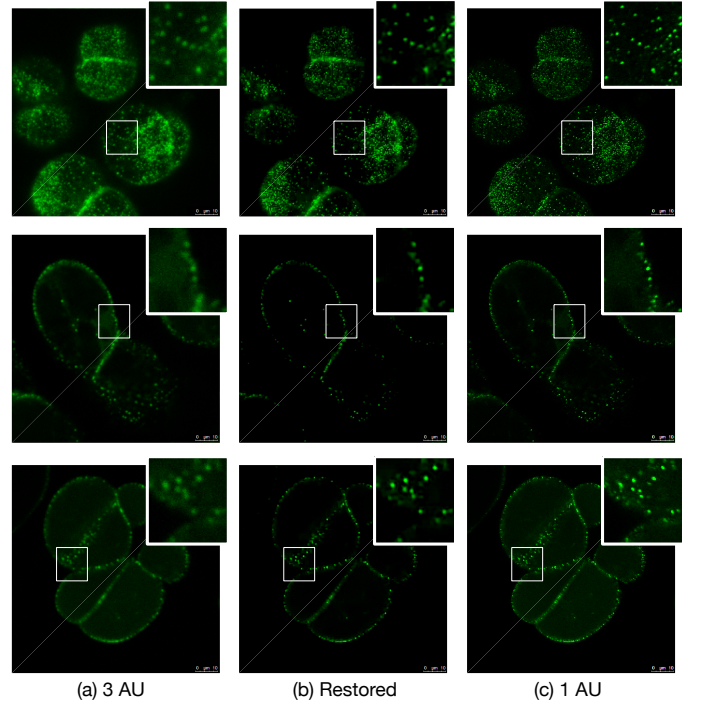


Fig. 14. Acquired and restored confocal fluorescence microscopy images of EXPOs [78]. (a) Acquired images with pinhole size 3AU; (b) Deconvolved images using the PURE-LET algorithm; (c) Acquired images with pinhole size 1AU as the pseudo ground truth.

Thanks to [2], we know that

$$\mathbb{E} \{ (\mathbf{H}\mathbf{x})^T \mathbf{F}(y) \} = \mathbb{E} \{ y^T \mathbf{F}^{-1}(y) - \sigma^2 \text{div} \{ \mathbf{F}^{-1}(y) \} \}.$$

Using this identity, we can then replace  $\mathbb{E} \{ (\mathbf{H}\mathbf{x})^T \mathbf{H}^{-T} \mathbf{F}(y) \}$  by

$$\mathbb{E} \{ y^T \mathbf{H}^{-T} \mathbf{F}^{-1}(y) - \sigma^2 \text{div} \{ \mathbf{H}^{-T} \mathbf{F}^{-1}(y) \} \}.$$

The other expression,  $\mathbb{E} \{ (\mathbf{H}\mathbf{x})^T \mathbf{H}^{-T} \mathbf{H}^{-1} y \}$ , can be obtained by substituting  $\mathbf{H}^{-1} y$  to  $\mathbf{F}(y)$  in that expression, which yields

$$\mathbb{E} \{ y^T \mathbf{H}^{-T} \mathbf{H}^{-1} y - \alpha \mathbf{1}^T \mathbf{H}^{-T} \mathbf{H}^{-1} y \} - \sigma^2 \text{Tr} \{ \mathbf{H}^{-T} \mathbf{H}^{-1} \}.$$

Note that we have used  $\{ \mathbf{H}^{-T} \mathbf{F}(y) \}^- = \mathbf{H}^{-T} \mathbf{F}^{-1}(y)$ .  $\square$

## ACKNOWLEDGMENT

The authors would like to thank Prof. Liwen Jiang and Prof. Juan Wang for the preparation of the biological samples and for their help on acquiring the confocal fluorescence microscopy images. They also would like to thank the anonymous reviewers for their useful suggestions.

## REFERENCES

- [1] A. Foi, M. Trimeche, V. Katkovnik, and K. Egiazarian, "Practical Poissonian-Gaussian noise modeling and fitting for single-image raw-data," *IEEE Trans. Image Process.*, vol. 17, no. 10, pp. 1737–1754, 2008.
- [2] F. Luisier, T. Blu, and M. Unser, "Image denoising in mixed Poisson-Gaussian noise," *IEEE Trans. Image Process.*, vol. 20, no. 3, pp. 696–708, 2011.
- [3] T. E. Nichols, J. Qi, E. Asma, and R. M. Leahy, "Spatiotemporal reconstruction of list-mode PET data," *IEEE Trans. Med. Imag.*, vol. 21, no. 4, pp. 396–404, 2002.

- [4] H. Lantéri and C. Theys, "Restoration of astrophysical images - The case of Poisson data with additive Gaussian noise," *EURASIP J. Adv. Signal Process.*, vol. 2005, no. 15, pp. 2500–2513, Sep. 2005.
- [5] C. Vonesch, F. Aguet, J.-L. Vonesch, and M. Unser, "The colored revolution of bioimaging," *IEEE Signal Process. Mag.*, vol. 23, no. 3, pp. 20–31, 2006.
- [6] D. L. Snyder, R. L. White, and A. M. Hammoud, "Image recovery from data acquired with a charge-coupled-device camera," *J. Opt. Soc. Am. A*, vol. 10, no. 5, pp. 1014–1023, May 1993.
- [7] E. Bratsolis and M. Sigelle, "A spatial regularization method preserving local photometry for Richardson-Lucy restoration," *Astronom. and Astrophys.*, vol. 375, no. 3, pp. 1120–1128, Sep. 2001.
- [8] L. A. Shepp and Y. Vardi, "Maximum likelihood reconstruction for Emission Tomography," *IEEE Trans. Med. Imag.*, vol. 1, no. 2, pp. 113–122, 1982.
- [9] T. Hohage and F. Werner, "Inverse problems with poisson data: statistical regularization theory, applications and algorithms," *Inverse Probl.*, vol. 32, no. 9, p. 093001, 2016.
- [10] P. Sarder and A. Nehorai, "Deconvolution methods for 3-D fluorescence microscopy images," *IEEE Signal Process. Mag.*, vol. 23, no. 3, pp. 32–45, 2006.
- [11] T. Kenig, Z. Kam, and A. Feuer, "Blind image deconvolution using machine learning for three-dimensional microscopy," *IEEE Trans. Pattern Anal. Mach. Intell.*, vol. 32, no. 12, pp. 2191–2204, 2010.
- [12] F. Conte, A. Germani, and G. Iannello, "A Kalman filter approach for denoising and deblurring 3-d microscopy images," *IEEE Trans. Image Process.*, vol. 22, no. 12, pp. 5306–5321, 2013.
- [13] H. Wang and P. C. Miller, "Scaled heavy-ball acceleration of the Richardson-Lucy algorithm for 3D microscopy image restoration," *IEEE Trans. Image Process.*, vol. 23, no. 2, pp. 848–854, 2014.
- [14] C. Kervrann, C. O. Sanchez Sorzano, S. T. Acton, J. C. Olivo Marin, and M. Unser, "A guided tour of selected image processing and analysis methods for fluorescence and electron microscopy," *IEEE J. Sel. Top. Sign. Process.*, vol. 10, no. 1, pp. 6–30, 2016.
- [15] M. Ponti, E. Helou, P. J. Ferreira, and N. Mascarenhas, "Image restoration using gradient iteration and constraints for band extrapolation," *IEEE J. Sel. Top. Sign. Process.*, vol. 10, no. 1, pp. 71–80, 2016.
- [16] J. Li, F. Luisier, and T. Blu, "PURE-LET deconvolution of 3D fluorescence microscopy images," in *Proc. IEEE Int. Symp. Biomed. Imaging (ISBI)*, 2017, pp. 723–727.
- [17] R. Neelamani, H. Choi, and R. Baraniuk, "ForWaRD: Fourier-wavelet regularized deconvolution for ill-conditioned systems," *IEEE Trans. Signal Process.*, vol. 52, no. 2, pp. 418–433, 2004.
- [18] K. Dabov, A. Foi, V. Katkovnik, and K. Egiazarian, "Image restoration by sparse 3D transform-domain collaborative filtering," *Proc. SPIE Electron. Imag.*, vol. 6812, pp. 701–712, 2008.
- [19] H. Takeda, S. Farsiu, and P. Milanfar, "Deblurring using regularized locally adaptive kernel regression," *IEEE Trans. Image Process.*, vol. 17, no. 4, pp. 550–563, 2008.
- [20] J. A. Guerrero-Colon, L. Mancera, and J. Portilla, "Image restoration using space-variant Gaussian scale mixtures in overcomplete pyramids," *IEEE Trans. Image Process.*, vol. 17, no. 1, pp. 27–41, 2008.
- [21] F. Xue, F. Luisier, and T. Blu, "Multi-Wiener SURE-LET deconvolution," *IEEE Trans. Image Process.*, vol. 22, no. 5, pp. 1954–1968, 2013.
- [22] M. A. T. Figueiredo and J. M. Bioucas-Dias, "Restoration of Poissonian images using alternating direction optimization," *IEEE Trans. Image Process.*, vol. 19, no. 12, pp. 3133–3145, 2010.
- [23] S. Lefkimmiatis and M. Unser, "Poisson image reconstruction with Hessian Schatten-Norm regularization," *IEEE Trans. Image Process.*, vol. 22, no. 11, pp. 4314–4327, 2013.
- [24] J. Salmon, Z. Harmany, C.-A. Deledalle, and R. Willett, "Poisson noise reduction with non-local PCA," *J. Math. Imaging. Vis.*, vol. 48, no. 2, pp. 279–294, 2014.
- [25] W. H. Richardson, "Bayesian-based iterative method of image restoration," *J. Opt. Soc. Am. A*, vol. 62, no. 1, pp. 55–59, 1972.
- [26] L. B. Lucy, "An iterative technique for the rectification of observed distributions," *The Astron. J.*, vol. 79, p. 745, 1974.
- [27] M. Bertero, P. Boccacci, G. Desiderà, and G. Vicidomini, "Image deblurring with Poisson data: from cells to galaxies," *Inverse Probl.*, vol. 25, no. 12, pp. 123006–27, 2009.
- [28] N. Dey, L. Blanc-Feraud, C. Zimmer, P. Roux, Z. Kam, J.-C. Olivo-Marin, and J. Zerubia, "Richardson-Lucy algorithm with total variation regularization for 3D confocal microscope deconvolution," *Microsc. Res. Tech.*, vol. 69, no. 4, pp. 260–266, 2006.
- [29] Z. T. Harmany, R. F. Marcia, and R. M. Willett, "This is SPIRAL-TAP: Sparse Poisson intensity reconstruction algorithms: theory and practice," *IEEE Trans. Image Process.*, vol. 21, no. 3, pp. 1084–1096, 2012.
- [30] A. Benfenati and V. Ruggiero, "Inexact Bregman iteration with an application to Poisson data reconstruction," *Inverse Probl.*, vol. 29, no. 6, p. 065016, 2013.
- [31] J. L. Starck and F. Murtagh, "Image restoration with noise suppression using the wavelet transform," *Astronom. and Astrophys.*, vol. 288, pp. 342–348, 1994.
- [32] R. D. Nowak and M. J. Thul, "Wavelet-vaguelette restoration in photon-limited imaging," *Proc. IEEE Int. Conf. Acoust. Speech Signal Process. (ICASSP)*, vol. 5, pp. 2869–2872, 1998.
- [33] A. Antoniadis and J. Bigot, "Poisson inverse problems," *Ann. Stat.*, vol. 34, no. 5, pp. 2132–2158, 2006.
- [34] M. Carlván and L. Blanc-Feraud, "Sparse Poisson noisy image deblurring," *IEEE Trans. Image Process.*, vol. 21, no. 4, pp. 1834–1846, 2012.
- [35] S. Setzer, G. Steidl, and T. Teuber, "Deblurring Poissonian images by split Bregman techniques," *J. Vis. Commun. Image R.*, vol. 21, no. 3, pp. 193–199, Apr. 2010.
- [36] N. Pastelnik and C. Chau, "Parallel proximal algorithm for image restoration using hybrid regularization," *IEEE Trans. Image Process.*, vol. 20, no. 9, pp. 2450–2462, 2011.
- [37] D.-Q. Chen, "Regularized generalized inverse accelerating linearized alternating minimization algorithm for frame-based Poissonian image deblurring," *SIAM J. Imaging Sci.*, vol. 7, no. 2, pp. 716–739, 2014.
- [38] F. X. Dupé, J. M. Fadili, and J. L. Starck, "A proximal iteration for deconvolving Poisson noisy images using sparse representations," *IEEE Trans. Image Process.*, vol. 18, no. 2, pp. 310–321, 2009.
- [39] R. Willett, "Multiscale analysis of photon-limited astronomical images," in *Proc. Stat. Challenges Mod. Astron. IV*, vol. 371, 2007, p. 247.
- [40] A. Rond, R. Giryes, and M. Elad, "Poisson inverse problems by the plug-and-play scheme," *J. Vis. Commun. Image Represent.*, vol. 41, pp. 96–108, 2016.
- [41] L. Ma, L. Moisan, J. Yu, and T. Zeng, "A dictionary learning approach for Poisson image deblurring," *IEEE Trans. Med. Imag.*, vol. 32, no. 7, pp. 1277–1289, 2013.
- [42] M. Mäkitalo and A. Foi, "Noise parameter mismatch in variance stabilization, with an application to Poisson-Gaussian noise estimation," *IEEE Trans. Image Process.*, vol. 23, no. 12, pp. 5348–5359, 2014.
- [43] —, "Optimal inversion of the generalized anscombe transformation for poisson-gaussian noise," *IEEE Trans. Image Process.*, vol. 22, no. 1, pp. 91–103, 2013.
- [44] Y. Le Montagner, E. D. Angelini, and J.-C. Olivo-Marin, "An unbiased risk estimator for image denoising in the presence of mixed Poisson-Gaussian noise," *IEEE Trans. Image Process.*, vol. 23, no. 3, pp. 1255–1268, 2014.
- [45] S. Yang and B.-U. Lee, "Poisson-Gaussian noise reduction using the hidden markov model in contourlet domain for fluorescence microscopy images," *PLoS One*, vol. 10, no. 9, p. e0136964, 2015.
- [46] F. Benvenuto, A. L. Camera, C. Theys, A. Ferrari, H. Lantéri, and M. Bertero, "The study of an iterative method for the reconstruction of images corrupted by Poisson and Gaussian noise," *Inverse Probl.*, vol. 24, no. 3, p. 035016, 2008.
- [47] J. Li, Z. Shen, R. Yin, and X. Zhang, "A reweighted L2 method for image restoration with Poisson and mixed Poisson-Gaussian noise," *Inverse Probl. Imag.*, vol. 9, no. 3, pp. 875–894, 2015.
- [48] E. Chouzenoux, A. Jezierska, J.-C. Pesquet, and H. Talbot, "A convex approach for image restoration with exact Poisson-Gaussian likelihood," *SIAM J. Imaging Sci.*, vol. 8, no. 4, pp. 2662–2682, 2015.
- [49] B. Baji, J. Lindblad *et al.*, "Blind restoration of images degraded with mixed Poisson-Gaussian noise with application in transmission electron microscopy," in *Proc. IEEE Int. Symp. Biomed. Imaging (ISBI)*, 2016, pp. 123–127.
- [50] Y. Marnissi, Y. Zheng, E. Chouzenoux, and J.-C. Pesquet, "A variational bayesian approach for image restoration. application to image deblurring with poisson-gaussian noise," *IEEE Trans. Comput. Imaging*, 2017, to appear.
- [51] V. Kempen and V. Vliet, "The influence of the regularization parameter and the first estimate on the performance of Tikhonov regularized non-linear image restoration algorithms," *J. Microsc.*, vol. 198, no. 1, pp. 63–75, 2000.
- [52] J. M. Bardsley and J. Goldes, "Regularization parameter selection methods for ill-posed Poisson maximum likelihood estimation," *Inverse Probl.*, vol. 25, no. 9, p. 095005, 2009.
- [53] M. Bertero, P. Boccacci, G. Talenti, R. Zanella, and L. Zanni, "A discrepancy principle for Poisson data," *Inverse Probl.*, vol. 26, no. 10, p. 105004, Oct. 2010.
- [54] A. Stagliano, P. Boccacci, and M. Bertero, "Analysis of an approximate model for poisson data reconstruction and a related discrepancy principle," *Inverse Probl.*, vol. 27, no. 12, p. 125003, 2011.

- [55] D.-Q. Chen and L.-Z. Cheng, "Spatially adapted regularization parameter selection based on the local discrepancy function for Poissonian image deblurring," *Inverse Probl.*, vol. 28, no. 1, p. 015004, 2012.
- [56] T. Blu and F. Luisier, "The SURE-LET approach to image denoising," *IEEE Trans. Image Process.*, vol. 16, no. 11, pp. 2778–2786, 2007.
- [57] F. Luisier, C. Vonesch, T. Blu, and M. Unser, "Fast interscale wavelet denoising of poisson-corrupted images," *Signal Process.*, vol. 90, no. 2, pp. 415–427, 2010.
- [58] M. Raphan and E. P. Simoncelli, "Optimal denoising in redundant representations," *IEEE Trans. Image Process.*, vol. 17, no. 8, pp. 1342–1352, 2008.
- [59] E. P. Simoncelli, "Bayesian denoising of visual images in the wavelet domain," in *Bayesian inference in wavelet-based models*. Springer, 1999, pp. 291–308.
- [60] J. Li, F. Luisier, and T. Blu, "Deconvolution of Poissonian images with PURE-LET approach," in *Proc. IEEE Int. Conf. Image Proc. (ICIP)*, 2016, pp. 2708–2712.
- [61] C. Vonesch and M. Unser, "A fast thresholded landweber algorithm for wavelet-regularized multidimensional deconvolution," *IEEE Trans. Image Process.*, vol. 17, no. 4, pp. 539–549, 2008.
- [62] J.-C. Pesquet, A. Benazza-Benyahia, and C. Chau, "A SURE approach for digital signal/image deconvolution problems," *IEEE Trans. Image Process.*, vol. 57, no. 12, pp. 4616–4632, 2009.
- [63] M. V. Afonso, J. M. Bioucas-Dias, and M. A. Figueiredo, "An augmented lagrangian approach to the constrained optimization formulation of imaging inverse problems," *IEEE Trans. Image Process.*, vol. 20, no. 3, pp. 681–695, 2011.
- [64] C. M. Stein, "Estimation of the mean of a multivariate normal distribution," *Ann. Stat.*, vol. 9, pp. 1135–1151, 1981.
- [65] D. L. Donoho and I. M. Johnstone, "Adapting to unknown smoothness via wavelet shrinkage," *J. Am. Stat. Assoc.*, vol. 90, no. 432, pp. 1200–1224, 1995.
- [66] J.-C. Pesquet and D. Leporini, "A new wavelet estimator for image denoising," in *Proc. 6th Int. Conf. Image Processing and Its Applications*, vol. 1. IET, 1997, pp. 249–253.
- [67] F. Luisier, T. Blu, and M. Unser, "A new SURE approach to image denoising: Interscale orthonormal wavelet thresholding," *IEEE Trans. Image Process.*, vol. 16, no. 3, pp. 593–606, 2007.
- [68] C. Chau, L. Duval, A. Benazza-Benyahia, and J.-C. Pesquet, "A nonlinear Stein-based estimator for multichannel image denoising," *IEEE Trans. Image Process.*, vol. 56, no. 8, pp. 3855–3870, 2008.
- [69] S. Ramani, T. Blu, and M. Unser, "Monte-Carlo SURE: A black-box optimization of regularization parameters for general denoising algorithms," *IEEE Trans. Image Process.*, vol. 17, no. 9, pp. 1540–1554, 2008.
- [70] A. Jezierska, C. Chau, J.-C. Pesquet, H. Talbot, and G. Engler, "An EM approach for time-variant poisson-gaussian model parameter estimation," *IEEE Trans. Signal Process.*, vol. 62, no. 1, pp. 17–30, 2014.
- [71] L. Azzari and A. Foi, "Indirect estimation of signal-dependent noise with nonadaptive heterogeneous samples," *IEEE Trans. Image Process.*, vol. 23, no. 8, pp. 3459–3467, 2014.
- [72] C. Sutour, C.-A. Deledalle, and J.-F. Aujol, "Estimation of the noise level function based on a nonparametric detection of homogeneous image regions," *SIAM J. Imaging Sci.*, vol. 8, no. 4, pp. 2622–2661, 2015.
- [73] M. Rakhshanfar and M. A. Amer, "Estimation of Gaussian, Poissonian-Gaussian, and processed visual noise and its level function," *IEEE Trans. Image Process.*, vol. 25, no. 9, pp. 4172–4185, 2016.
- [74] J. L. Starck, J. Fadili, and F. Murtagh, "The undecimated wavelet decomposition and its reconstruction," *IEEE Trans. Image Process.*, vol. 16, no. 2, pp. 297–309, 2007.
- [75] M. Arigovindan, J. C. Fung, D. Elnatan, V. Mennella, Y.-H. M. Chan, M. Pollard, E. Branlund, J. W. Sedat, and D. A. Agard, "High-resolution restoration of 3D structures from widefield images with extreme low signal-to-noise-ratio." *Proc. Natl. Acad. Sci. U.S.A.*, vol. 110, no. 43, pp. 17 344–17 349, Oct. 2013.
- [76] R. Zanello, G. Zanghirati, R. Cavicchioli, L. Zanni, P. Boccacci, M. Bertero, and G. Vicidomini, "Towards real-time image deconvolution: application to confocal and STED microscopy," *Sci. Rep.*, vol. 3, p. 2523, Aug. 2013.
- [77] A. Wong, X. Y. Wang, and M. Gorbet, "Bayesian-based deconvolution fluorescence microscopy using dynamically updated nonstationary expectation estimates," *Sci. Rep.*, vol. 5, p. 10849, Jun. 2015.
- [78] J. Wang, Y. Ding, J. Wang, S. Hillmer, Y. Miao, S. W. Lo, X. Wang, D. G. Robinson, and L. Jiang, "EXPO, an exocyst-positive organelle distinct from multivesicular endosomes and autophagosomes, mediates cytosol to cell wall exocytosis in arabidopsis and tobacco cells," *Plant Cell.*, vol. 22, no. 12, pp. 4009–4030, 2010.
- [79] B. Zhang, J. Zerubia, and J.-C. Olivo-Marin, "Gaussian approximations of fluorescence microscope point-spread function models," *Appl. Opt.*, vol. 46, no. 10, pp. 1819–1829, 2007.
- [80] J. Boulanger, C. Kervrann, P. Bouthemy, P. Elbau, J.-B. Sibarita, and J. Salamero, "Patch-based nonlocal functional for denoising fluorescence microscopy image sequences," *IEEE Trans. Med. Imag.*, vol. 29, no. 2, pp. 442–454, 2010.
- [81] J. Li, F. Xue, and T. Blu, "Fast and accurate three-dimensional point spread function computation for fluorescence microscopy," *J. Opt. Soc. Am. A*, vol. 34, no. 6, pp. 1029–1034, 2017.